A General Framework for Computing the Turbulence Structure Tensors

F.S. Stylianou[a], R. Pecnik[b], S.C. Kassinos[a,*]

[a] *Computational Sciences Laboratory (UCY-CompSci), Department of Mechanical and Manufacturing Engineering, University of Cyprus, Kallipoleos Avenue 75, Nicosia 1678, Cyprus*
[b] *Process & Energy Department, Delft University of Technology, Leeghwaterstraat 39, 2628CB, Delft, The Netherlands*

Abstract

Good measures of the turbulence structure are important for turbulence modeling, flow diagnostics and analysis. Structure information is complementary to the componentality anisotropy that the Reynolds stress tensor carries, and because structures extend in space, structure information is inherently non-local. Given access to instantaneous snapshots of a turbulence field or two-point statistical correlations, one can extract the structural features of the turbulence. However, this process tends to be computationally expensive and cumbersome. Therefore, one-point statistical measures of the structural characteristics of turbulence are desirable. The *turbulence structure tensors* are one-point statistical descriptors of the non-local characteristics of the turbulence structure and form the mathematical framework for constructing Structure-Based Models (SBM) of turbulence. Despite the promise held by SBM, the tensors have so far been available only in a small number of DNS databases of rather simple canonical flows. This inhibits further SBM development and discourages the use of the tensors for flow analysis and diagnostics. The lack of a clear numerical recipe for computing the tensors in complex domains is one the reasons for the scarce reporting of the structure tensors in DNS databases. In particular, the imposition of proper boundary conditions in complex geometries is non-trivial. In this work, we provide for the first a time a rigorous and well-documented description of a mathematical and computational framework that can be used for the calculation of the structure tensors in arbitrary turbulent flow configurations.

*Corresponding author
Email addresses: stylianou.fotos@ucy.ac.cy (F.S. Stylianou), kassinos@ucy.ac.cy (S.C. Kassinos)

Keywords: structure tensors, stream vector, complex domains, multiply-connected, turbulent flow, turbulence structures.

1. Introduction

1.1. Background

Far from being equivalent to white noise, the turbulent motion of fluids is organized in the form of coherent structures, often given the label 'eddies'. In high Reynolds number flows, the size of the turbulence eddies can span several orders of magnitude. In these flows, the small-scale structure is thought to be effectively shielded from external forcing and thus exhibits a significant degree of isotropy as a result. It is further assumed that the role of the smaller eddies is primarily to dissipate the turbulence energy. The larger energy-containing structures, on the other hand, are both shaped by and play a role in determining the response of turbulence to external deformation. They are dynamically active. The footprint of these large energy-containing turbulence eddies is reflected in the turbulence statistics. Quantitative measures of turbulence structure are easily constructed using two-point correlations, but such descriptions tend to be rather costly and impractical for engineering application, which relies heavily on one-point formulations. Hence, one-point measures of turbulence structure are needed. Kassinos and Reynolds [15] were the first to develop a comprehensive one-point mathematical formulation that can be used to quantify different aspects of the energy containing turbulence structures. They proceeded to propose the use of the one-point turbulence structure tensors in turbulence modeling and for flow diagnostics, which they described in [7, 15, 16]. In this regard, they showed that it is possible for two turbulence fields to share the same *componentality* state, i.e. to have the same Reynolds stress tensor values, but yet have different underlying turbulence structure. Differences in the turbulence structure, although undetectable through the componentality information, lead to different dynamic behavior of the turbulence, for example in response to external deformation. Hence, a complete one-point description of the turbulence requires the information contained in the structure tensors. Namely, the structure *dimensionality* D_{ij} gives information about the directions of independence in the turbulence, the structure *circulicity* F_{ij} gives information on the large scale circulation in the flow, and the *inhomogeneity* C_{ij} gives the degree of inhomogeneity of the turbulence. The third-rank *stropholysis* Q_{ijk} becomes important when mean rotation breaks the reflectional symmetry of the turbulence. Exact definitions of these tensors are given in the next section.

One-point turbulence models that use only the Reynolds stresses and the turbulence scales to characterize the turbulence are fundamentally incomplete [15]. This applies to both simple eddy-viscosity closures and to Reynolds Stress Transport (RST) models and it is particularly problematic when the mean deformation includes strong mean or frame rotation. For example, in this case, the dynamic response of nearly isotropic turbulence is very different from that of turbulence with strongly organized two-dimensional structures and turbulence models should be able to distinguish between the two. Without ad hoc modifications, most turbulence closures, however, fail to do that because they are insensitive to the structural characteristics of the turbulence. Furthermore, turbulence models should incorporate the breaking of reflectional symmetry whenever mean or frame rotation can dynamically affect the flow (flow through axisymmetric diffuser or nozzle with swirl, flow through turbomachinery). These aforementioned effects are nonlocal in nature, yet they can be addressed via the one-point structure tensors, which is the main feature of the tensors that makes them particularly attractive in engineering practice.

Structure-Based turbulence Models (SBMs) [11, 13, 15, 16, 20] are a class of turbulence models that make use of the one-point turbulence tensors. SBMs hold promise for resolving some of the limitations described above. However, an obstacle in the further development of structure-based models has been the relatively scarce availability of data from simulations and experiments that could be used for model validation. On one hand, the one-point structure tensors are not easily available from experiments. Hence, one normally has to turn to direct (DNS) or large eddy simulations (LES) for obtaining data on the tensors. Even in this case, however, the specification of proper boundary conditions for the computation of the structure tensors has so far been considered only in the simplest geometries, e.g. fully-developed channel flow and free shear flows [16]. The underlying ambiguity over how one can compute the tensors in complex domains has discouraged the more widespread inclusion of the tensors in turbulence databases. This in turn has hurt the development of structure-based models and also prevented the more widespread use of the tensors as flow diagnostics. As SBM testing and validation progresses to complex flow configurations this limitation becomes more pressing.

The purpose of this work is to present a clear framework for the numerical computation

of the structure tensors in arbitrarily complex geometries using DNS or LES data. We believe that this contribution will encourage the inclusion of the structure tensors in DNS databases, thus accelerating the development of structure-based models and encouraging the use of one-point structure tensors as flow diagnostic tools.

1.2. Definition of the Structure Tensors

The structure tensors are determined through the turbulent stream vector ψ_i', defined by the equations [16]

$$u_i' = \epsilon_{ijk}\psi_{k,j}' \qquad \psi_{k,k}' = 0 \qquad \psi_{i,kk}' = -\omega_i' \,, \tag{1}$$

where u_i' and ω_i' are the fluctuating velocity and vorticity components, and ϵ_{ijk} is the Levi-Civita alternating tensor. To complete the stream vector definition suitable boundary conditions must be supplied. Hereafter, a comma followed by an index denotes partial differentiation with respect to the implied coordinate direction. The Einstein summation convention is implied on repeated Roman, but not on Greek indices. Note that ψ_i' satisfies a Poisson equation and hence carries non-local information. As will be shown, the divergence-free condition on ψ_i' is important for the physical meaning of the resulting structure tensors. The focus of this paper is a general strategy for solving (1) in complex domains, thus making possible the computation of the structure tensors in practical flow configurations.

Expressing the definition of the Reynolds stresses in terms of the fluctuating stream vector,

$$R_{ij} = \overline{u_i' u_j'} = \epsilon_{ipq}\epsilon_{jrs}\overline{\psi_{q,p}'\psi_{s,r}'} \,, \tag{2}$$

and using the identity

$$\epsilon_{ipq}\epsilon_{jrs} = \det \begin{pmatrix} \delta_{ij} & \delta_{ir} & \delta_{is} \\ \delta_{pj} & \delta_{pr} & \delta_{ps} \\ \delta_{qj} & \delta_{qr} & \delta_{qs} \end{pmatrix} \,, \tag{3}$$

leads to the constitutive relation

$$R_{ij} + D_{ij} + F_{ij} - (C_{ij} + C_{ji}) = \delta_{ij} q^2 \,, \tag{4}$$

where $q^2 = R_{kk} = 2k$ is twice the turbulent kinetic energy. Based on this equation, the

second-rank structure tensors are defined as

$$\text{Componentality} \qquad R_{ij} = \overline{u_i' u_j'} \qquad r_{ij} = R_{ij}/R_{kk} \qquad \tilde{r}_{ij} = r_{ij} - \delta_{ij}/3 \tag{5a}$$

$$\text{Dimensionality} \qquad D_{ij} = \overline{\psi_{k,i}' \psi_{k,j}'} \qquad d_{ij} = D_{ij}/D_{kk} \qquad \tilde{d}_{ij} = d_{ij} - \delta_{ij}/3 \tag{5b}$$

$$\text{Circulicity} \qquad F_{ij} = \overline{\psi_{i,k}' \psi_{j,k}'} \qquad f_{ij} = F_{ij}/F_{kk} \qquad \tilde{f}_{ij} = f_{ij} - \delta_{ij}/3 \tag{5c}$$

$$\text{Inhomogeneity} \qquad C_{ij} = \overline{\psi_{i,k}' \psi_{k,j}'} \qquad c_{ij} = C_{ij}/D_{kk} \qquad \tilde{c}_{ij} = c_{ij} - c_{kk}\delta_{ij}/3\,. \tag{5d}$$

Unlike the other structure tensors, the inhomogeneity C_{ij} is not positive semi-definite and thus the trace $C_{kk} = D_{kk} - R_{kk}$ can be negative or even zero. For this reason, C_{ij} is normalized in terms of the trace $D_{kk} = F_{kk}$. Another possibility would have been to normalize all structure tensors with the trace R_{kk}, but this choice is ill-defined on solid boundaries, where R_{kk} is zero. On the contrary, D_{kk} is nonzero at the walls and proves to be the most meaningful choice for normalizing all the structure tensors.

A detailed discussion of the physical meaning of each structure tensor is given in [16], but the key features are recounted here. While the structure tensors carry complementary information, the constitutive equation provides a linear dependence among them, thus any one of the tensors can be reconstructed if the rest are known. The *componentality* R_{ij} (the Reynolds stress tensor) gives information about which components of the fluctuating velocity are more energetic. The *dimensionality* D_{ij} carries information about the directions of independence of the turbulence. This can be easily seen based on the definition of D_{ij}, since gradients of the stream vector tend to vanish along directions of strong structure elongation and tend to be strongest along directions in which short structures are stacked. The *circulicity* F_{ij} defines the directions with large-scale circulation concentrated around them. Finally, the *inhomogeneity* C_{ij} gives the directions of inhomogeneity of the turbulence. In fact, the inhomogeneity tensor vanishes identically in homogeneous flows, as can be shown by recasting the inhomogeneity definition into the form

$$C_{ij} = (\overline{\psi_i' \psi_{k,j}'})_{,k} - \overline{\psi_i' \psi_{k,kj}'}\,. \tag{6}$$

Here, the first term is zero only in homogeneous flows, while the second term is always zero due to the specific choice $\psi_{k,k} = 0$. The inhomogeneity is significant near solid boundaries and relaxes to zero far away from them. At intermediate distances form the wall, the magnitude

of C_{ij} becomes small compared to that of the other structure tensors. Since little is known on how to model C_{ij} in general flows, structure-based turbulence models, such as the Algebraic Structure-Based Model (ASBM) [2, 14, 17, 22], are based on the *homogenized* tensors. These are obtained by absorbing C_{ij} inside D_{ij} and F_{ij},

$$D^{cc}_{ij} \equiv D_{ij} - \frac{1}{2}(C_{ij} + C_{ji}) \qquad F^{cc}_{ij} \equiv F_{ij} - \frac{1}{2}(C_{ij} + C_{ji})\,. \tag{7}$$

Note, that the homogenized tensors now satisfy $D^{cc}_{kk} = F^{cc}_{ii} = R_{ii} = q^2$.

To complete the one-point tensorial base, an additional third rank structure tensor must be defined because one can show that it carries information that is not contained in the second-rank tensors,

$$Q_{ijk} = -\overline{u'_j \psi'_{i,k}} = \epsilon_{jrs}\overline{\psi'_{r,s}\psi'_{i,k}}\,. \tag{8}$$

Using the definitions of the second-rank structure tensors, one can show that

$$\epsilon_{imp}Q_{mjp} = R_{ij} \qquad Q_{ikj} - Q_{jki} = \epsilon_{ijp}R_{pk} \tag{9a}$$

$$\epsilon_{imp}Q_{pmj} = D_{ij} - C_{ij} \qquad Q_{jik} - Q_{ijk} = \epsilon_{ijp}(D_{pk} - C_{pk}) \tag{9b}$$

$$\epsilon_{imp}Q_{jpm} = F_{ij} - C_{ji} \qquad Q_{kji} - Q_{kij} = \epsilon_{ijp}(F_{pk} - C_{kp})\,. \tag{9c}$$

The homogenized tensors can also be calculated from the third rank tensor,

$$D^{cc}_{ij} = \frac{1}{2}(\epsilon_{imp}Q_{pmj} + \epsilon_{jmp}Q_{pmi}) \qquad F^{cc}_{ij} = \frac{1}{2}(\epsilon_{imp}Q_{jpm} + \epsilon_{jmp}Q_{ipm})\,. \tag{10}$$

A third-rank constitutive equation connects all the structure tensors,

$$Q_{ijk} = \frac{1}{6}\epsilon_{ijk}q^2 + \frac{1}{3}\epsilon_{ikp}R_{pj} + \frac{1}{3}\epsilon_{jip}(D_{pk} - C_{pk}) + \frac{1}{3}\epsilon_{kjp}(F_{pi} - C_{ip}) + Q^*_{ijk}\,, \tag{11}$$

where the *Stropholysis* tensor

$$Q^*_{ijk} = \frac{1}{6}(Q_{ijk} + Q_{jik} + Q_{jki} + Q_{kji} + Q_{ikj} + Q_{kij}) \tag{12}$$

is the fully symmetric part of the third rank structure tensor. Stropholysis literally means "breaking by rotation" to bear in mind that this tensor remains zero in turbulence that has been deformed only by irrotational mean strain. However, mean and frame rotation break the reflectional symmetry of turbulence and generate Q^*_{ijk}. Once generated, the stropholysis

can be further modified by irrotational mean strain [15]. It is worth noting that the bi-traces of the third rank tensor are

$$Q_{kik} = 0 \qquad Q_{kki} = Q_{ikk} = -(\overline{u'_k \psi'_i})_{,k} \qquad Q^*_{kik} = Q^*_{kki} = Q^*_{ikk} = -\frac{2}{3}(\overline{u'_k \psi'_i})_{,k}\,, \tag{13}$$

which all vanish in homogeneous turbulence.

1.3. The Interpretation of the Structure Tensors

An idealized schematic representation of various types of eddies, along with the corresponding state of the structure tensors is shown in Fig. 1. For example, as shown in Fig. 1a, a state of $d_{11} = 0$, $r_{11} = 0$ and $f_{11} = 1$ means that the large scale structures are 2D eddies aligned with x_1 axis, with motion confined in planes perpendicular to the x_1 axis, and circulation concentrated on the axis of independence. We call this type of structures *vortical* eddies. On the other hand, the case $d_{11} = 0$, $r_{11} = 1$ and $f_{11} = 0$ corresponds to 2D eddies with motion confined along the x_1 axis, and no circulation on the axis of independence. We call these structures *jetal* eddies. The case $d_{11} = 0$, $r_{11} = a$ and $f_{11} = 1 - a$, corresponds to 2D eddies with helical type of motion.

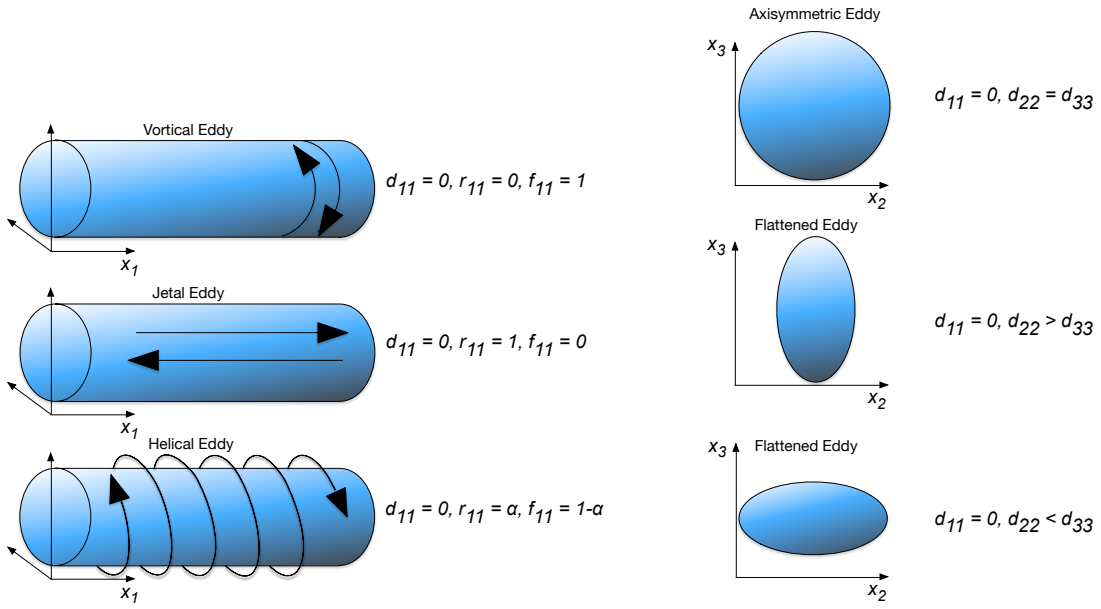

(a) (b)

Figure 1: *Schematic of idealized eddies showing the interpretation of the structure tensors. (a) three types of elongated eddies aligned with the x_1 axis and the corresponding values of the structure tensors: vortical eddy (top) is 2D-2C, jetal eddy (middle) is 2D-1C and helical eddy (bottom) is 2D-3C; (b) the dimensionality tensor also reflects the flattening of the eddy cross section.*

In addition, the eddies can be *flattened* instead of axisymmetric, as for example happens under the action of mean rotation, and this is also reflected in the state of the structure tensors, as shown in Fig. 1b. When the turbulence eddies are completely flattened, they become sheets or pancake turbulence [16] (a term coined by W.C. Reynolds), as shown in Fig. 2. In this case, the turbulence becomes 1D with the direction normal to the pancakes being the sole direction of dependence. The turbulence can be 1D-1C, as shown in Fig. 2, and these different states are properly captured by the structure tensors.

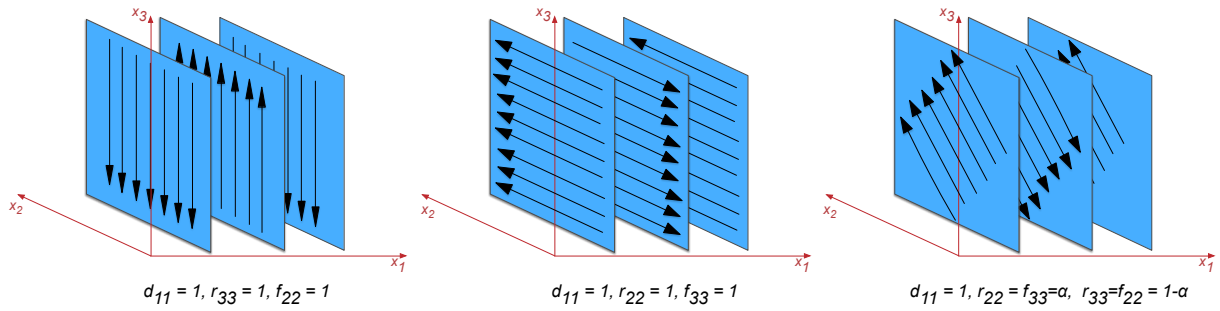

(a) (b) (c)

Figure 2: *Schematic of idealized sheets (pancake turbulence) showing the interpretation of the structure tensors. (a) 1D-1C turbulence that depends only on the x_1 axis, with fluctuating motion aligned with the x_3 axis and producing large-scale circulation around the x_2 axis; (b) same as in (a), but the motion is along the x_2 axis and large-scale circulation is around the x_3 axis; (c) 1D-1C, with the fluctuating motion within the sheets being at an angle relative to the plane axes.*

So far, the discussion has been limited to idealized structures for the sake of clarity. Nevertheless, it is important to appreciate that these idealizations correspond to structures that have been observed in various DNS of both homogeneous and inhomogeneous turbulence. The case of homogeneous magnetohydrodynamic (MHD) turbulence offers a nice example of this. Under the action of an external magnetic field at low magnetic Reynolds numbers, MHD turbulence can be driven close to the idealized 2D and 1D states depicted in Figs. 1 and 2. Fig. 3 shows results from a 256^3 DNS of homogeneous MHD turbulence sheared in fixed and rotating frames [12]. The simulations were performed at low magnetic Reynolds number ($R_m = 1$) and medium magnetic interaction number ($N = 10$). In this class of flows, the evolution of the turbulence structure is determined by the relative magnitudes of three characteristic time scales, that of the mean shear (τ_{shear}), magnetic diffusion (τ_m) and frame rotation ($\tau_{\text{rot}} = 1/\Omega^f$). In the particular case shown in Fig. 3, the three time scales were comparable ($\tau_{\text{shear}} = 2\tau_m = \tau_{\text{rot}}/2$), which means that all three effects were contributing to the deformation of the turbulence structure.

In this regard, it is revealing to examine the structure tensors for large values of the total shear. Specifically, we want to examine the structure tensors as late as possible given the size of the computational box. This ensures that the external forcing had the chance to shape the turbulence structure. Table 1 summarizes the values of turbulence structure

tensors computed from the DNS simulation for the same instant of time as the contour plots of Fig. 3. The mean shear tends to elongate the structures in the streamwise direction x_1, while the external magnetic field tends to elongate the structures in its own direction of alignment, x_3. Because in this case the two effects act over similar characteristic time scales ($M = 2$), the result is that the turbulence is deformed into thin horizontal sheets that are stacked on top of each other in the x_2 direction. This is reflected in the corresponding values of the structure tensors in Table 1, namely $d_{11} \approx d_{33} \to 0$ and $d_{22} \to 1$. In direct analogy to the schematic of Fig. 2c, motion is confined in these jetal sheets ($r_{11} \approx r_{33} \gg r_{22}$), which produces large scale circulation about the x_1 and x_3 axes ($f_{11} \approx f_{33} \gg f_{22}$). A completely different structure is obtained when the turbulence is deformed in a rotating frame (Fig. 3b). In this case, at large times the turbulence is driven into a state characterized by vertical slabs normal to the spanwise direction ($d_{11} \approx d_{22} \to 0$ and $d_{33} \to 1$). These structural slabs correspond to jetal motion primarily in the x_1 and to a lesser extent in the x_2 direction ($r_{11} > r_{22} \gg r_{33}$). As a result, in this case large-scale circulation is concentrated primarily around the x_2 axis and to lesser extent around the x_1 axis ($f_{22} > f_{11} \gg f_{33}$).

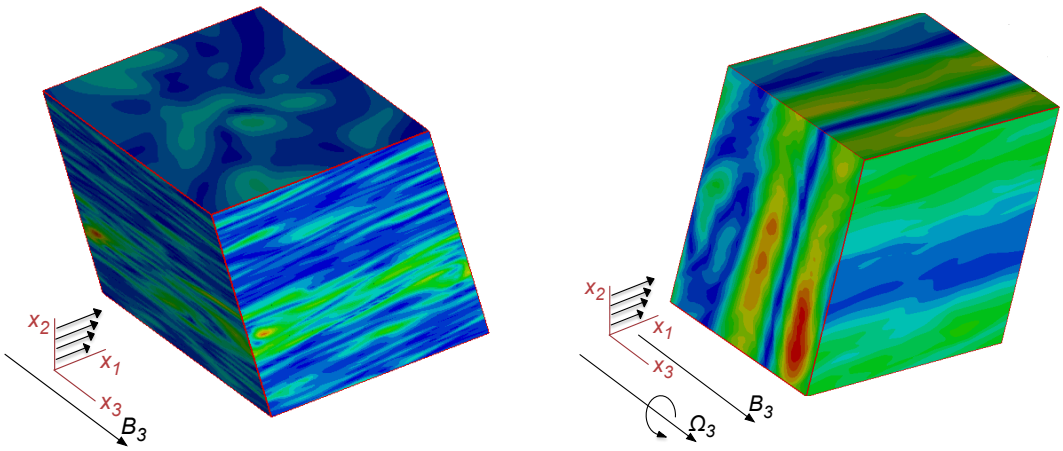

Figure 3: *DNS results for homogeneous shear ($dU_1/dx_2 = S$) of MHD turbulence under the action of a uniform spanwise external magnetic field (B_3) at low magnetic Reynolds number ($Re_m = 1$, $N = 10$). Two cases are considered: (a) shear in fixed frame and (b) shear in a frame rotating about the spanwise (Ω_3). Velocity magnitude contours taken at large total shear show remarkable structural differences between the two cases, which are captured by the structure tensors (Table 1).*

Case	r_{11}	r_{22}	r_{33}	d_{11}	d_{22}	d_{33}	f_{11}	f_{22}	f_{33}
Fixed frame	0.5	0.08	0.42	0.12	0.86	0.12	0.38	0.18	0.44
Rotating frame	0.61	0.39	0.0	0.0	0.02	0.98	0.38	0.58	0.04

Table 1: *One-point structure tensor components corresponding to the contour plots of Fig. 3*

1.4. The Structure Tensors in Inhomogeneous Flows

The behavior of the structure tensors for homogeneous and inhomogeneous turbulence subjected to various modes of mean deformation was reported by [16]. It is worth noting that the only case of wall-bounded turbulence that they considered was that of fully-developed channel flow. In this section, we review the main results from the channel flow simulations in order to demonstrate the ability of the structure tensors to describe the structure of wall-bounded turbulent flows.

Consider a fully-developed channel flow where $\hat{\boldsymbol{e}}_1$ is in streamwise direction, $\hat{\boldsymbol{e}}_2$ is in wall normal inhomogeneous direction and, $\hat{\boldsymbol{e}}_3$ is in spanwise homogeneous direction. For low $Re_\tau = \frac{u_\tau H}{\nu} \leq 385$ (based on the wall shear velocity u_τ, and channel half-width H), the results of [16] (Figure 13 therein) show that the d_{11} is smaller than d_{22}, and d_{33} throughout the channel. This indicates the presence of large-scale structures that are preferentially elongated in the streamwise direction. Thus, the picture painted by the structure tensors is consistent with the presence of streaks, quasi-streamwise vortices, large scale and very large-scale structures that have been observed experimentally and numerically.

In fact, the structure tensors can be used to discern more details. In the near-wall region ($y^+ < 5$), the values of the structure tensors indicate that the near-wall structures are almost 2-D ($d_{11} \to 0$), aligned with the wall ($d_{12} \to 0$), have roughly circular cross-section ($d_{22} \approx d_{33}$), have a strong jetal character ($r_{11} \gg r_{33} > r_{22}$, $r_{12} \to 0$), and with little circulation around their axes ($f_{11} \to 0$). The properties of these structures, as given by the structure tensors, are suggestive of the streaky structures that are known to exist in the near-wall region of turbulent channel flows. As one moves away from the wall, d_{11} gains value, but it still remains significantly lower than d_{22} and d_{33}, which points to quasi-elongated structures in the streamwise direction. In the same area, f_{11} also increases significantly above its almost zero near-wall value. Thus, away from the wall the turbulence structure contains

not only jetal, but also vortical motion about the elongated axis. In fact, these structures are best described as being of the helical type, since neither a strong vortical ($f_{11} \neq 0$), nor a strong jetal character ($r_{11} \neq 1$) predominates on the structures.

In the near wall region ($y^+ < 30$), the degree of inhomogeneity is strong and this is reflected in the high values attained by the c_{22} component of the inhomogeneity tensor. However, in the log-low region the inhomogeneity is almost zero indicating that the flow is locally homogeneous. This is in agreement with [23], where local homogeneity in the log-region has been noted.

2. A Discrepancy is Noted

Based on the preceding discussion, one should be able to appreciate the ability of the structure tensors to describe qualitatively and quantitatively the structure of turbulent flows. Before proceeding further, we need to point out a problem with the method previously used in literature for computing the structure tensors. For example, in the case of fully-developed channel flow, the stream vector boundary conditions used in [16] are given by

$$\hat{\boldsymbol{n}} \times \boldsymbol{\psi}|_S = 0 \qquad \boldsymbol{\nabla} \cdot \boldsymbol{\psi}|_S = 0. \tag{14}$$

However, careful scrutiny of the velocity field reconstructed from the resulting stream vector reveals a constant offset relative to the original velocity field. The constant shift does not affect the values of the structure tensor components since these involve only the fluctuating part of the velocity field. Thus, the structure tensor values reported by [16] were correct. Nevertheless, despite the fortuitous recovery of the correct result, this discrepancy suggests that the set of boundary conditions (14) are not quite appropriate.

To clarify this issue further, we have used the aforementioned boundary conditions (14) in order to compute the stream vector in a DNS of fully-developed pipe flow at $Re_b = u_b D/\nu = 5300$ (based on the bulk velocity u_b, and pipe diameter D) using a streamwise domain of $15R$, where R is the pipe radius. The results are shown in Fig. 4, where the reconstructed streamwise velocity is found again to be offset by a constant. The offset is not a turbulent effect; it exists also in a laminar fully-developed pipe flow.

As will be shown later, the cause of the spurious velocity offset is the inappropriate use of the boundary conditions in (14), which are strictly appropriate only in the case of

simply connected domains. However, periodic domains, such as those used for fully-developed channel and pipe flow, are multiply connected. In simple geometries, such as those considered so far, the inappropriate use of (14) results only in an inconsequential constant offset in the velocity field. The use of (14) in the case of complex, multiply connected, domains is much more problematic (i.e. boundary conditions (14) are derived only for wall velocity boundaries).

Based on this discussion, it is obvious that a much more careful handling of the stream vector boundary conditions is needed in order to compute the turbulence structure tensors in flow domains of arbitrary complexity.

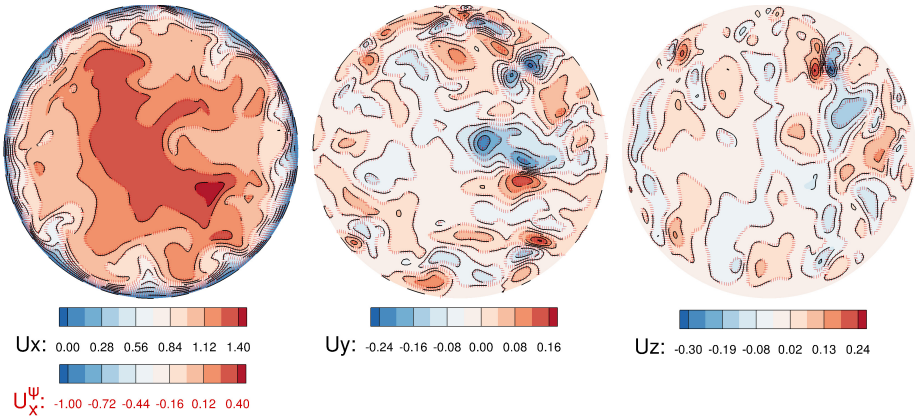

Figure 4: *fully-developed turbulent flow in a pipe at* $Re_b = 5300$. *At random instant and for a random cross section of the pipe, the velocity contours in conjunction with their respective iso-lines are shown. The original velocity components are represented by black dashed lines, while those reconstructed from the stream vector are illustrated with red dotted lines. The contour levels for the streamwise reconstructed velocity are off by a constant shift.*

3. Mathematical Framework

3.1. Foundation of the Framework

By definition, the evaluation of the structure tensors involves the computation of the stream vector. While a vast amount of information is available in the literature for the solution of *two-dimensional* flows using the vorticity/stream-function formulation, the three-dimensional vorticity/stream-vector problem has not received a comparable attention. Here, we provide the mathematical framework that allows the computation of the structure tensors in three-dimensional flows for both simply and multiply connected domains. The method we

have developed is based on the treatment of the three-dimensional vorticity/stream-vector problem by L. Quartapelle, who describes three alternative solution strategies, including appropriate boundary conditions [21]. Only two of these methods are suitable for use with the structure tensors. The first of the two can be used in only simply connected domains, while the second is also applicable to multiply connected domains.

3.2. The Vorticity Equation

Even though we do not need to solve the differential transport equation for the vorticity, it is important to bear in mind its origin. Recalling the definition of vorticity

$$\boldsymbol{\omega} = \boldsymbol{\nabla} \times \boldsymbol{u} \tag{15}$$

and by taking the curl of the momentum equations, the vorticity equation follows

$$\frac{\partial \boldsymbol{\omega}}{\partial t} + \boldsymbol{\nabla} \times (\boldsymbol{\omega} \times \boldsymbol{u}) = \nu \nabla^2 \boldsymbol{\omega}. \tag{16}$$

As an initial condition for this equation one should use

$$\boldsymbol{\omega}|_{t=0} = \boldsymbol{\nabla} \times \boldsymbol{u}|_{t=0}. \tag{17}$$

By the definition of vorticity it follows that it must be solenoidal at all times, $\boldsymbol{\nabla} \cdot \boldsymbol{\omega} = 0$. To guarantee the satisfaction of such a property it is sufficient to enforce the divergence-free condition only on the boundary. This can be shown by taking the divergence of vorticity equation, which gives

$$\frac{\partial (\boldsymbol{\nabla} \cdot \boldsymbol{\omega})}{\partial t} = \nu \nabla^2 (\boldsymbol{\nabla} \cdot \boldsymbol{\omega}), \tag{18}$$

with the initial condition $\boldsymbol{\nabla} \cdot \boldsymbol{\omega}|_{t=0} = \boldsymbol{\nabla} \cdot \boldsymbol{\nabla} \times \boldsymbol{u}|_{t=0} = 0$. If the homogeneous boundary condition

$$\boldsymbol{\nabla} \cdot \boldsymbol{\omega}|_S = 0 \tag{19}$$

is also supplied, then the solution of the differential equation at any time will be $\boldsymbol{\nabla} \cdot \boldsymbol{\omega} = 0$. Thus, it will prove useful to keep in mind the following equations that apply to the vorticity vector,

$$\frac{\partial \boldsymbol{\omega}}{\partial t} = -\boldsymbol{\nabla} \times (\boldsymbol{\omega} \times \boldsymbol{u}) + \nu \nabla^2 \boldsymbol{\omega} \tag{20a}$$

$$\boldsymbol{\omega}|_{t=0} = \boldsymbol{\nabla} \times \boldsymbol{u}|_{t=0} \tag{20b}$$

$$\boldsymbol{\nabla} \cdot \boldsymbol{\omega}|_S = 0. \tag{20c}$$

Two additional boundary conditions are needed to uniquely define the vorticity. As shown by Quartapelle [21], the stream vector has five boundary conditions, two of which can be recast into vorticity integral conditions.

3.3. Stream Vector Formulation

In general, any vector field can be decomposed into a divergence free part and an irrotational part (Helmholtz decomposition),

$$\boldsymbol{u} = \boldsymbol{\nabla}\phi + \boldsymbol{\nabla} \times \boldsymbol{\psi}. \tag{21}$$

The decomposition is not unique until boundary conditions are prescribed. Since for incompressible flows the velocity field is solenoidal, we can define the stream vector according to

$$\boldsymbol{u} = \boldsymbol{\nabla} \times \boldsymbol{\psi}. \tag{22}$$

From the velocity boundary condition $\boldsymbol{u}|_S = \boldsymbol{u}^S$ (arbitrary case), it follows that $\boldsymbol{\nabla} \times \boldsymbol{\psi}|_S = \boldsymbol{u}^S$, where the superscript "S" signifies the boundary surface. Separating the tangential and normal components of this boundary condition, we get

$$\hat{\boldsymbol{n}} \times \boldsymbol{\nabla} \times \boldsymbol{\psi}|_S = \hat{\boldsymbol{n}} \times \boldsymbol{u}^S \qquad \hat{\boldsymbol{n}} \cdot \boldsymbol{\nabla} \times \boldsymbol{\psi}|_S = \hat{\boldsymbol{n}} \cdot \boldsymbol{u}^S, \tag{23}$$

where $\hat{\boldsymbol{n}}$ is the normal vector on the boundary. A partial differential equation for the stream vector follows from (15) and (22),

$$\boldsymbol{\nabla} \times \boldsymbol{\nabla} \times \boldsymbol{\psi} = \boldsymbol{\omega}. \tag{24}$$

The differential equation (24) and the boundary condition (23) do not define $\boldsymbol{\psi}$ uniquely. This is a consequence of the invariance of (22) to gauge transformations of the form

$$\boldsymbol{\psi} \to \boldsymbol{\psi} + \boldsymbol{\nabla}\theta, \tag{25}$$

where θ is an arbitrary scalar function. This gauge freedom allows additional conditions on $\boldsymbol{\psi}$. One can impose the Euclid (or Coulomb) gauge condition,

$$\boldsymbol{\nabla} \cdot \boldsymbol{\psi} = 0, \tag{26}$$

which implies that (24) is equivalent to

$$-\nabla^2 \boldsymbol{\psi} = \boldsymbol{\omega}. \tag{27}$$

On the other hand, since $\boldsymbol{\nabla} \cdot \boldsymbol{\omega} = 0$, it follows from (27) that

$$\nabla^2 (\boldsymbol{\nabla} \cdot \boldsymbol{\psi}) = 0. \tag{28}$$

Provided that the boundary condition $\boldsymbol{\nabla} \cdot \boldsymbol{\psi}|_S = 0$ is enforced, the Euclid gauge condition is automatically satisfied at all times.

The Euclid gauge condition still does not define uniquely the stream vector. The gradient of any scalar function θ that satisfies the Laplace equation $\nabla^2 \theta = 0$ can be added to the stream vector (see (25)), which will continue to satisfy the Euclid gauge condition. Therefore, one must specify additional conditions on the stream vector. As a result of (25), for any such condition that is imposed, $\boldsymbol{\nabla}\theta$ must satisfy a corresponding homogeneous condition. Homogeneous boundary conditions on θ lead to a solution of $\theta = 0$ everywhere in the domain, and therefore the uniqueness of the stream vector is evident. The different gauge conditions that can be chosen for the remaining condition lead to different stream vector formulations. In the following sections, we discuss two such formulations based on the work of Quartapelle [21].

To summarize we have the following set of equations that uniquely define the stream vector,

$$\begin{aligned}
-\nabla^2 \boldsymbol{\psi} &= \boldsymbol{\omega} && \text{(29a)} \\
\hat{\boldsymbol{n}} \times \boldsymbol{\nabla} \times \boldsymbol{\psi}|_S &= \hat{\boldsymbol{n}} \times \boldsymbol{u}^S && \text{(29b)} \\
\hat{\boldsymbol{n}} \cdot \boldsymbol{\nabla} \times \boldsymbol{\psi}|_S &= \hat{\boldsymbol{n}} \cdot \boldsymbol{u}^S && \text{(29c)} \\
\boldsymbol{\nabla} \cdot \boldsymbol{\psi}|_S &= 0 && \text{(29d)} \\
&\text{plus an extra gauge condition.} && \text{(29e)}
\end{aligned}$$

It is evident that we have more than three boundary conditions for the stream vector. As shown by Quartapelle, some of them are satisfied automatically whenever equations from (29) are used for eliciting suitable (integral) conditions for the vorticity (these are the missing conditions from equations (20)).

3.4. Formulation for Simply Connected Domains

In the case of simply connected domains, the as-yet-undetermined gauge condition (29e) can be used to specify the tangential components of the stream vector at the boundary surface of the domain. As shown by Quartapelle, the resulting formulation for the stream vector is well-posed and can be summarized as

$$-\nabla^2\boldsymbol{\psi} = \boldsymbol{\omega} \tag{30a}$$

$$\hat{\boldsymbol{n}}\times\boldsymbol{\psi}|_S = \hat{\boldsymbol{n}}\times\boldsymbol{a} \qquad \left[\boldsymbol{a} = -\hat{\boldsymbol{n}}\times\boldsymbol{\nabla}_S q^S + \boldsymbol{\nabla}_S p^S \qquad -\nabla_S^2 q^S = \hat{\boldsymbol{n}}\cdot\boldsymbol{u}^S\right] \tag{30b}$$

$$\boldsymbol{\nabla}\cdot\boldsymbol{\psi}|_S = 0, \tag{30c}$$

where $\boldsymbol{\nabla}_S$ is the surface gradient operator and ∇_S^2 is the surface Laplacian (or Laplace-Beltrami) operator. The tangential components of the stream vector at the boundary are defined by means of the solution to a surface elliptic problem. The solution of the surface problem specifies the scalar function q^S, which in-turn fixes the tangent component of the stream vector at the boundary. The scalar function p^S is instead arbitrary and can be set to zero without loss of generality. One does not need to specify boundary conditions for the surface problem since the surface of a 3D domain does not have boundaries. The proof for the above formulation holds only for simply connected domains[1]. One can solve analytically the above equations in a fully-developed laminar pipe flow (simply connected domain with specified inlet/outlet conditions).

3.5. Formulation for Multiply Connected Domains

In multiply connected domains, a well-posed formulation is obtained if the free gauge condition (29e) is used for specifying the normal component of the stream vector [21]. Without going into details, the resulting formulation is defined by the equations

$$-\nabla^2\boldsymbol{\psi} = \boldsymbol{\omega} \tag{31a}$$

$$\hat{\boldsymbol{n}}\cdot\boldsymbol{\psi}|_S = a_n^S \qquad \left[\oint a_n^S \mathrm{d}S = 0\right] \tag{31b}$$

$$\hat{\boldsymbol{n}}\times\boldsymbol{\nabla}\times\boldsymbol{\psi}|_S = \hat{\boldsymbol{n}}\times\boldsymbol{u}^S, \tag{31c}$$

[1]Even though the current formulation is for simply connected domains, it can be used for the calculation of the structure tensors in multiply connected domains as well. Since for us the velocity field is considered as known, we can use the current formulation in multiply connected spaces by splitting the domain into smaller parts that are simply connected.

where $a_n^S = \psi_n^S(\boldsymbol{x}^S, t)$ is an arbitrary scalar function defined on the boundary S that satisfies the integral constraint of (31b). A valid choice for a_n^S is simply zero everywhere on the boundary surface. One can solve analytically the above equations in a fully-developed laminar pipe flow (periodic domain in the streamwise direction).

3.6. Gauge Invariance

The development of the formulations for simply and multiply connected domains was based on the Euclid gauge condition that was chosen in section 3.3. The development was presented without offering sufficient justification for this particular choice. In this section, we show that imposing the Euclid gauge condition is in fact needed in order to ensure the gauge invariance of the structure tensors. Furthermore, this particular choice instills a number of desirable properties to the structure tensors.

The Reynolds stress tensor R_{ij} is gauge invariant and it is desirable that the remaining structure tensors satisfy this property as well. To clarify the issue of gauge invariance, we will focus on the particular example of the structure dimensionality tensor D_{ij}. If we allow for the gauge transformation of the stream vector $\psi_i^\theta = \psi_i + \theta_{,i}$, then D_{ij} transforms according to

$$\begin{aligned} D_{ij}^{\psi^\theta} &\equiv \overline{\psi'^{\theta}_{k,i}\psi'^{\theta}_{k,j}} \\ &= \overline{\psi^\theta_{k,i}\psi^\theta_{k,j}} - \overline{\psi^\theta_{k,i}}\;\overline{\psi^\theta_{k,j}} \\ &= D_{ij}^{\psi} + (\overline{\psi_{k,i}\theta_{,kj}} - \overline{\psi_{k,i}}\;\overline{\theta_{,kj}}) + (\overline{\psi_{k,j}\theta_{,ki}} - \overline{\psi_{k,j}}\;\overline{\theta_{,ki}}) + (\overline{\theta_{,ki}\theta_{,kj}} - \overline{\theta_{,ki}}\;\overline{\theta_{,kj}})\,. \end{aligned} \quad (32)$$

Thus, in this form the structure dimensionality, and as one can show the remaining structure tensors as well, depends not only on the stream vector field, but on the gauge θ as well. This is undesirable as it introduces an element of ambiguity in the interpretation of the individual tensors. The simplest approach that removes the dependence on the gauge is to impose the Euclid gauge condition $\psi_{i,i} = 0$, as has already been done in section 3.3. The Euclid gauge condition implies that the scalar function θ must satisfy the Laplace equation $\nabla^2\theta = 0$. Any additional gauge boundary conditions applied on the stream vector imply a homogeneous time-independent boundary condition for θ. Hence, the Euclid gauge condition results in a time-independent solution for θ, which in turn causes all the parenthetical terms in (32) to vanish and renders the structure-tensors gauge independent.

Furthermore, the particular choice of the Euclid gauge imparts a number of additional desirable properties to the structure tensors, namely:

- the inhomogeneity tensor C_{ij} becomes identically zero in homogeneous flows,
- a simple relation connects the circulicity spectrum tensor to the vorticity spectrum tensor in homogeneous flows,
- equation (24) reduces to (27),
- a set of recursive relations between ψ_i, u_i, ω_i become possible.

This discussion points to the fact that the Euclid gauge condition appears to be the natural one to impose.

4. Numerical Framework

4.1. Computational Procedure

The three-dimensional vorticity/stream-vector problem as defined by Quartapelle [21] is in general very complicated to be solved. The solution strategies of [21] involve deferential equations for six fields, the components of vorticity and stream vector, which are coupled. In our case, however, we are only interested in calculating the turbulence structure tensors in the context of velocity-pressure formulation that is commonly used in CFD codes. The vorticity needed in the stream vector Poisson equations is calculated through the velocity field. Therefore, only the stream vector formulation is used from the vorticity/stream-vector problem defined by L. Quartapelle. To make this point clear, one uses the following procedure at each time step for computing the structure tensors:

(a) calculate the velocity field via a velocity-pressure formulation,
(b) calculate the vorticity field through the velocity field,
(c) construct the proper boundary conditions and differential equations for the stream vector, using the previously calculated velocity and vorticity fields,
(d) calculate the stream vector field,
(e) calculate the structure tensors (collection of statistics is implied).

4.2. Treatment of the Poisson Differential Equations

In a velocity-pressure formulation, the stream vector can be treated as three passive scalars, since it does not affect the flow field. Thus, any CFD code can be modified to calculate the stream vector Poisson equations. One simply has to extract from the underlying CFD code the discretization scheme of the velocity diffusion term, and adopt it for the Poisson equations of the stream vector. In our case, we have adapted the finite volume method and the SBP (summation-by-parts) operators used in [9] to discretize the Laplacian operator. The numerics are described in detail in Appendix A.

For the discretization of the stream vector Poisson equations, we use the standard Cartesian coordinates (instead of curvilinear coordinates). This is a necessity if we want to develop a numerical scheme that is applicable in any geometry. Any geometry can be meshed with unstructured elements that are defined only in Cartesian coordinates. Furthermore the stream vector Poisson equations are decoupled in Cartesian coordinates. To elaborate this further, in the vector equation $-\nabla^2\boldsymbol{\psi} = \boldsymbol{\omega}$ the unit curvilinear vectors (that compose $\boldsymbol{\psi}$) are also subject to the derivatives of the Laplace operator, while the unit Cartesian vectors are not.

4.3. Treatment of the Boundary Conditions

The treatment of the boundary terms depends on the type of domain under consideration (i.e. simply connected vs multiply connected). Here, we proceed with the implementation of the boundary conditions for multiply connected domains since this represents the more general case. A complication arises since the boundary conditions (31b) and (31c) are coupled. We provide two ways to apply the boundary conditions: (a) the coupled form, and (b) the segregated form. The coupled form is suitable for solving the stream-vector components concurrently, while the segregated form is appropriate for an iterative solution procedure. In the coupled form, all stream vector components are solved at the same time. This means that at each boundary node a 3×3 sub-matrix is built. In the segregated form, the components are solved one at a time, and therefore an iterative procedure within each time step is needed in order to satisfy exactly the boundary conditions. The coupled form has faster convergence than the segregated, but also needs more memory (depending on the implementation it needs

more that 3 and less that 9 times the memory used by the segregated method) to store the linear system of equations to be solved.

For both coupled and segregated methods, we rearrange the boundary conditions (31b) and (31c), so that the normal gradient appears explicitly,

$$n_j \psi_j|_S = 0 \tag{33a}$$

$$-\boldsymbol{n}\cdot\boldsymbol{\nabla}\psi_i|_S = -n_j \frac{\partial \psi_j}{\partial x_i}\Big|_S + \epsilon_{ijk} n_j u_k^S, \qquad (i=1,2,3)\,, \tag{33b}$$

where $\boldsymbol{n}\cdot\boldsymbol{\nabla} = n_j \frac{\partial}{\partial x_j}$. Without loss of generality we have set $a_n^S = 0$. The above equations are four and thus one might think that the boundary conditions are overdetermined. Fortunately, the set of the three equations (33b) are not independent; they satisfy the scalar relation

$$n_i \left(-\boldsymbol{n}\cdot\boldsymbol{\nabla}\psi_i|_S + n_j \frac{\partial \psi_j}{\partial x_i}\Big|_S \right) = n_i \epsilon_{ijk} n_j u_k^S = 0. \tag{34}$$

This leaves us with three independent boundary conditions, (33a) and two from (33b). It should be noted that in the limit where $|n_\alpha| \to 1$, the α component of (33b) becomes trivial ($0 = 0$). For this reason, we always drop the α component of (33b) for which the $|n_\alpha|$ is maximum.

In the coupled method, we expand (33a) and (33b) to get

$$n_\alpha \psi_\alpha|_S + n_\beta \psi_\beta|_S + n_\gamma \psi_\gamma|_S = 0 \tag{35a}$$

$$-\boldsymbol{n}\cdot\boldsymbol{\nabla}\psi_\beta|_S = -n_j \frac{\partial \psi_j}{\partial x_\beta}\Big|_S + \epsilon_{\beta jk} n_j u_k^S \tag{35b}$$

$$-\boldsymbol{n}\cdot\boldsymbol{\nabla}\psi_\gamma|_S = -n_j \frac{\partial \psi_j}{\partial x_\gamma}\Big|_S + \epsilon_{\gamma jk} n_j u_k^S\,, \tag{35c}$$

where Greek indices are not subject to the summation convention. Index α corresponds to the maximum absolute component of the normal boundary surface vector (i.e. $|n_\alpha| > |n_\beta|, |n_\gamma|$), while the remaining indices, β and γ, are such that a right handed coordinate system is formed. All the components of the stream vector appearing both in the left and right hand side of (35) are treated implicitly (i.e. they are considered unknown).

In the segregated method, we use the Euclid gauge condition to rewrite (33a) and (33b)

into a form that is more suitable for the iterative procedure used in each time step,

$$\psi_\alpha|_S = -\frac{n_\beta}{n_\alpha}\psi_\beta|_S - \frac{n_\gamma}{n_\alpha}\psi_\gamma|_S \tag{36a}$$

$$-\boldsymbol{n}\cdot\boldsymbol{\nabla}\psi_\beta|_S = \epsilon_{\alpha jk}n_j\frac{\partial\psi_\gamma}{\partial x_k}\Big|_S - \epsilon_{\gamma jk}n_j\frac{\partial\psi_\alpha}{\partial x_k}\Big|_S + \epsilon_{\beta jk}n_j u_k^S \tag{36b}$$

$$-\boldsymbol{n}\cdot\boldsymbol{\nabla}\psi_\gamma|_S = \epsilon_{\beta jk}n_j\frac{\partial\psi_\alpha}{\partial x_k}\Big|_S - \epsilon_{\alpha jk}n_j\frac{\partial\psi_\beta}{\partial x_k}\Big|_S + \epsilon_{\gamma jk}n_j u_k^S\,. \tag{36c}$$

In each of the three equations (36), the right hand side is independent of the stream vector component appearing on the left and depends only on the remaining two components. Thus, all components of the stream vector appearing on the right hand side can be treated explicitly (i.e. they are considered known) and their values are taken from the previous iteration. In the case of the first iteration, values from the previous time step are used to initiate the iterative sequence.

4.4. Other Numerical Aspects

For the coupled solution procedure, the linear system of Poisson equations is only built once. Only the boundary conditions are applied at each time step, since they depend on the instantaneous velocity field. The performance of the coupled algorithm depends: (a) on the arrangement of the algebraic equations and (b) the iterative method used to solve the linear system of equations. We use the matrix arrangement of [6] (section 7 therein). The PETSc package [3, 4, 5] is used for solving the coupled system of equations. By experimenting with various solver options available in PETSc, we have concluded that the Generalized Minimal Residual (GMRES) iterative Krylov subspace method, in conjunction with either the left preconditioning additive Schwarz method (PCASM) or with block Jacobi preconditioning (PCBJACOBI), gives acceptable convergence speed.

Once the instantaneous stream vector has been calculated, the structure tensors are computed by collecting statistics. The structure tensors are defined through the fluctuating stream vector and the fluctuating velocity vector. Using the relations

$$u_i' = u_i - \overline{u_i} \tag{37a}$$

$$\psi_i' = \psi_i - \overline{\psi_i}, \tag{37b}$$

we can rewrite the structure tensors into the following form,

$$R_{ij} = \overline{u'_i u'_j} = \overline{u_i u_j} - \overline{u_i}\ \overline{u_j} \tag{38a}$$

$$D_{ij} = \overline{\psi'_{k,i}\psi'_{k,j}} = \overline{\psi_{k,i}\psi_{k,j}} - \overline{\psi_{k,i}}\ \overline{\psi_{k,j}} \tag{38b}$$

$$F_{ij} = \overline{\psi'_{i,k}\psi'_{j,k}} = \overline{\psi_{i,k}\psi_{j,k}} - \overline{\psi_{i,k}}\ \overline{\psi_{j,k}} \tag{38c}$$

$$C_{ij} = \overline{\psi'_{i,k}\psi'_{k,j}} = \overline{\psi_{i,k}\psi_{k,j}} - \overline{\psi_{i,k}}\ \overline{\psi_{k,j}} \tag{38d}$$

$$Q_{ijk} = -\overline{u'_j\psi'_{i,k}} = -(\overline{u_j\psi_{i,k}} - \overline{u_j}\ \overline{\psi_{i,k}})\,. \tag{38e}$$

As a result of the no-slip boundary condition ($u_i^{wall} = 0$ at stationary wall boundaries) it follows that $Q_{ijk}^{wall} = 0$ and $R_{ij}^{wall} = 0$. However, the same does not necessarily hold true for the stream vector, i.e. in general $\psi_i^{wall} \neq 0$, and thus in general, D_{ij}^{wall}, F_{ij}^{wall}, C_{ij}^{wall} assume nonzero values at the wall. Nevertheless, one can show that $D_{ij}^{wall} = F_{ij}^{wall} = C_{ij}^{wall}$.

The numerical discretization scheme provided in this paper for the Poisson equations is second order (see Appendix A). The discretization of the tangential (to the surface boundary) components of the boundary sub-face gradient operator is second order, while its normal component is only first order. This is not an issue since the internal grid points adjacent to the boundaries are always very close to the borders of the computational domain due to viscous limitations (usually a distance of 1/2 wall units is acceptable).

The third rank tensor Q_{ijk} uses the gradients of the stream vector and the fluctuating velocity, while the other tensors uses the gradients of the stream in power two. Therefore, Q_{ijk} carries smaller numerical errors. All the second-rank tensors can either be calculated directly through the definitions (38) or through tensorial contraction of Q_{ijk} with the Levi-Civita alternating tensor. The later method is preferable as it is less prone to numerical errors carried by the gradient of the stream vector.

5. Validation of the Implementation

The flow around a circular cylinder placed symmetrically in a plane channel is an ideal test case for the stream vector implementation. This is true for the following reasons: (a) the domain is multiply connected, (b) this is a canonical flow covered extensively in scientific literature, (c) the vorticity/stream function formulation has been developed to solve two dimensional two component (2D-2C) flows around bluff bodies, (d) it is a simple test case

that involves the most commonly used velocity boundary conditions (walls, prescribed inlet, convective outlet, and zero normal gradient).

In what follows, we use velocity data from [10] to compute the stream vector. For the discretization of the associated differential equations we use the method of Appendix A, while the boundary conditions are treated as in section 4.3. A comparison of the original and reconstructed velocity (computed from the stream vector), validates the implementation of the stream-vector.

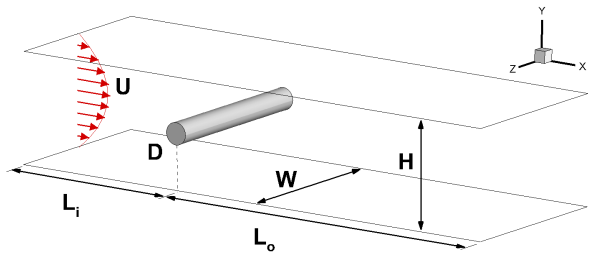

Figure 5: *Schematic diagram of the flow configuration and related geometrical parameters. Reproduction from [10].*

A schematic illustration of the flow configuration is given in Fig. 5. The geometry consists of a circular cylinder of diameter D, placed symmetrically in a plane channel. The origin of the coordinate system is placed in the middle of the cylinder. The ratio of the cylinder diameter D, to the channel height H, defines the blockage ratio $\beta = \frac{D}{H}$, which in this case is set to $\beta = \frac{1}{5}$. The inlet is located at a distance of $L_i = 12.5D$ upstream of the cylinder, while the outlet is placed at a downstream distance of $L_o = 35.5D$. The spanwise length of the channel and cylinder is $W = 8D$.

A Poiseuille parabolic velocity profile is prescribed at the inlet, while at the outlet a convective boundary condition is applied. A no-slip boundary condition is imposed on the cylinder surface, the top and bottom walls. A Neumann boundary condition has been adopted for the velocity field in the spanwise direction. A detailed description of the flow configuration, boundary condition and computational mesh is given in [10].

The Reynolds number $Re_c = U_c D/\nu$ (based on the cylinder diameter and the inlet centerline velocity) is used to classify the flow regimes. At $Re_c = 120$, the flow is laminar but unsteady, with vortices shed from the cylinder, giving rise to the well known von Kármán

vortex street. This flow regime serves our first validation since it is effectively 2D-2C. Fig. 6a shows the contour plots of the magnitude of the spanwise vorticity. Obtained at a random instant of the flow sequence, these plots reflect the vortex shedding process. Fig. 6b shows the active component of the stream vector ψ_z computed using the framework described above. Figs. 6c and 6d show the streamwise, u_x, and transverse, u_y, velocity components respectively. In these plots, the black dashed lines and the dotted red lines represent the original and reconstructed velocities respectively. The reconstructed and original velocity components coincide.

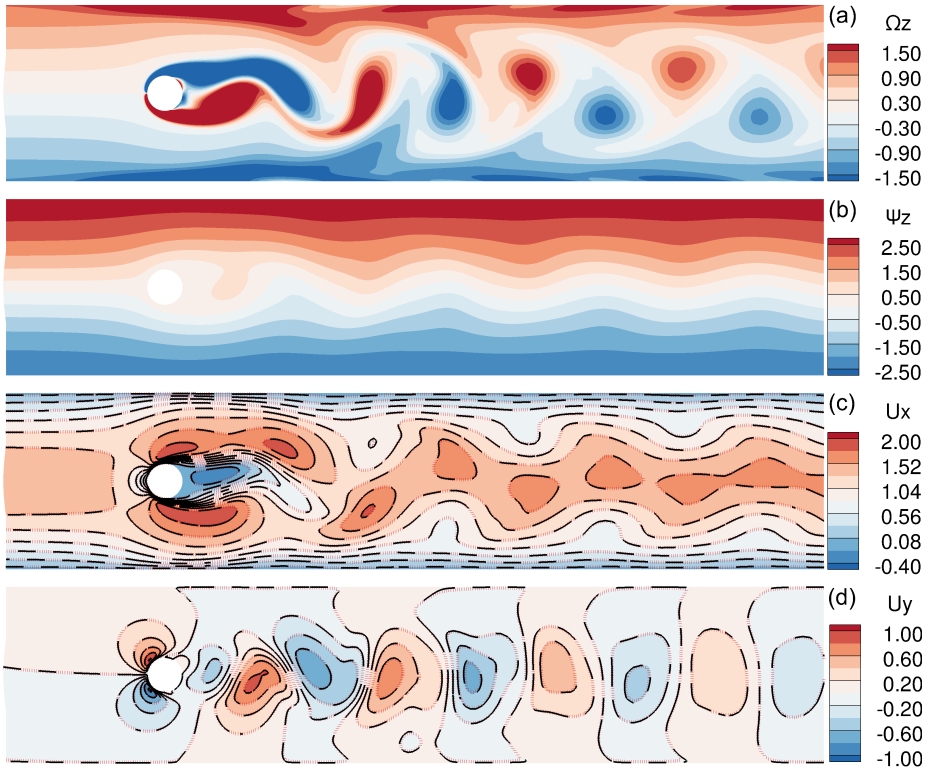

Figure 6: *Flow around a cylinder at* $Re_c = 120$. *Contour plots of vorticity, the non-zero components of the stream vector and velocity fields are shown. The flow is 2-D and thus at a random instant any* $z = const.$ *describes completely the flow. To enhance the flow characteristics part of the domain is shown; the x coordinate is restricted in the region* $x \in [-4.5D, 18.5D]$. *The velocity contour plots contain also their respective iso-lines. The original velocity components are represented by black dashed lines, while the stream vector reconstructed velocities are illustrated with red dotted lines.*

At $Re_c = 330$ the flow is in the transitional regime and the ensuing mode A instabilities change the character of the flow from a 2D-2C to a 3D-3C state. In this regime, the primary

vortex cores (spanwise rollers) are distorted by the formation of the streamwise vortex pairs. Depending on their characteristics, these secondary vortices they are classified into mode A and mode B instabilities (for more information see [10] and references therein). At $Re_c = 330$, the flow is dominated by mode B instabilities. This case will serve as our second validation case. Since the flow is 3D, three different slices suffice to validate the implementation. Figs. 7, 8, 9 correspond to slices ($z = 0, y = 0, x = 4D$ respectively) taken at a random instant in time. Velocity magnitude contours plots are shown in conjunction with the respective iso-lines. The dashed black lines and the dotted red lines represent the original and reconstructed velocities. It is clear that the velocities reconstructed using the stream vector coincide with the original ones for all three slices.

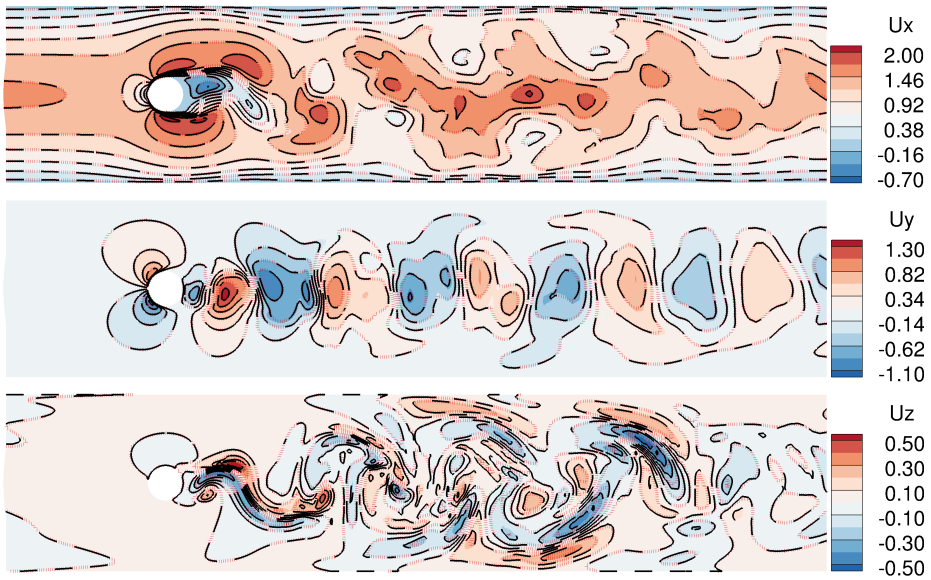

Figure 7: *Flow around a cylinder at $Re_c = 330$. For a random instant and at $z = 0$ the velocity contours in conjunction with their respective iso-lines are shown. To enhance the flow characteristics part of the domain is shown; the x coordinate is restricted in the region $x \in [-4.5D, 18.5D]$. The original velocity components are represented by black dashed lines, while the stream vector reconstructed velocities are illustrated with red dotted lines.*

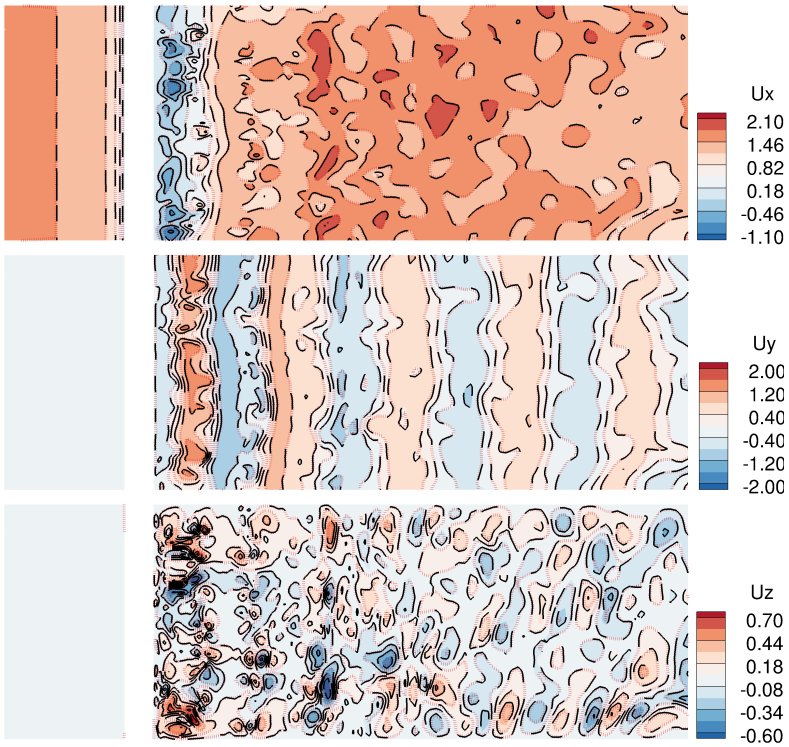

Figure 8: *Same as Fig. 7 but for the plane* $y = 0$.

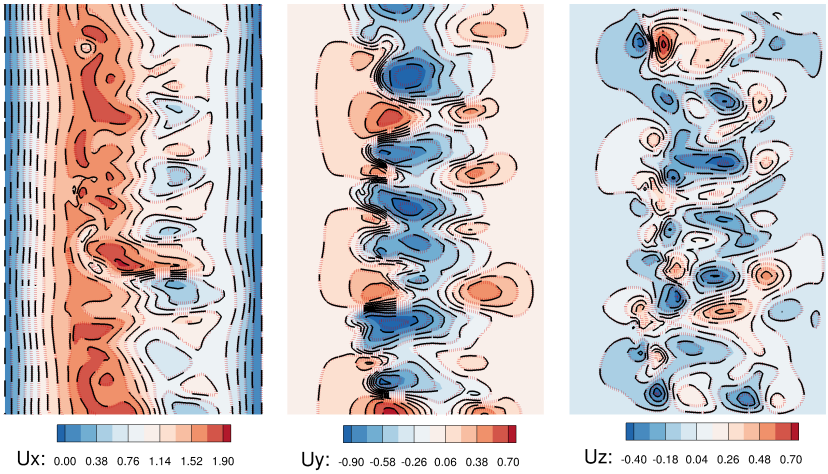

Figure 9: *Same as Fig. 7 but for the plane* $x = 4D$. *The direction of the flow is towards the reader.*

6. Conclusions

A complete and consistent mathematical and numerical framework for the computation of the one-point structure tensors has been presented. The framework presented can be used to obtain the stream vector in turbulent flow involving arbitrary geometries, which is a prerequisite for the computation of the structure tensors. We are already using the method described herein to compute the turbulence structure tensors in a number of complex flow configurations, including the case of developing turbulent flow through bifurcating pipe. We hope that the information made available herein will encourage other workers in the field to include the one-point structure tensors in their databases of complex turbulent flow cases. This in turn will provide a significant boost to the efforts of various teams to develop structure-based models (SBM) of turbulence, and will encourage the use of the tensors in the diagnosis of turbulent flow.

7. Acknowledgments

This work has been supported by the Cyprus Research Promotion Foundation through the Framework Programme for Research, Technological Development and Innovation 2009-2010 (ΔEΣMH 2009-2010) under Grant KOYΛTOYPA/BENΣ/0510/01. The support of the US Army International Technology Center and the US Air Force European Office of Aerospace Research and Development (EOARD) under grant W911NF-11-1-0425 is also gratefully acknowledged.

The authors wish to express their sincere gratitude to Prof. Luigi Quartapelle for his insightful comments on this paper and for providing the updated version (unpublished) of his monograph [21]. Finally, the authors gratefully acknowledge Dr. Nikolas Kanaris for providing the DNS data used in section 5.

Appendix A. Numerical Implementation of the Stream Vector Formulation

In this section, we describe the implementation of the stream vector formulation in the unstructured collocated nodal-based finite-volume code (CDP) that we use as the main platform for our CFD computations. In CDP, a second-order accurate centered-difference scheme, with skewness corrections, is applied to discretize the diffusive and nonlinear terms. The incompressibility condition and momentum equation are coupled using a fractional-step method. The time integration of the flow equations is done using a Crank-Nicholson scheme for the diffusive terms. The non-linear terms are treated semi-implicitly. A very detailed description of the numerical techniques used by this code is reported in [1, 8, 9, 18, 19, 24]. Numerical aspects that are important for the implementation of the stream vector formulation will be reported here also.

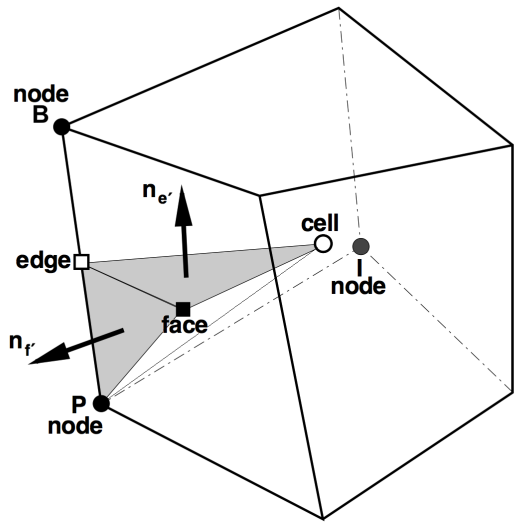

Figure A.1: *A typical unstructured grid element. Variable fields are stored at the nodes. One edge, one face and the cell center are illustrated. One sub-tet associated with node P, and its sub-edge and sub-face are shaded. Sub-faces are only used if the node P is a boundary node. Figure is modified from [9].*

A typical unstructured grid element is illustrated in Fig. A.1. Each mesh element is divided in sub-tetrahedrons (sub-tets), each of which is constructed by a node, an edge, a face and a cell. One such sub-tet, associate with node P, is sketch in Fig. A.1. The location of edges, faces and cells are calculated based on simple averages of their associated nodes. Since field variables are stored on nodes, simple averages are used also for the calculation of

the field variables at edges, faces and cells. The finite volume, node-based method implies the construction of the dual mesh. In the dual mesh, the-node based control volumes are centered around each node (vertices of the original grid). Therefore, the control volume for each node P, is made out by combining the appropriate sub-tets. Note that in Fig. A.1 not all neighbors of node P are shown, and thus only one fraction of its total volume can be constructed from the visible neighbors.

The volume integration of vorticity (right hand side of the stream vector Poisson equations) is discretized as

$$\int_P \omega_i dV \approx \sum_{t' \in T'_P} V_{t'} \omega_i^P, \tag{A.1}$$

where t' is an index for the sub-tets, $V_{t'}$ is the volume of the sub-tet t', and T'_P is the total number of sub-tets associated with P. The vorticity at node P is approximated using the discrete analog of its definition,

$$\begin{aligned}
\omega_i^P &= \frac{1}{V_P}\int_P \omega_i dV \\
&= \frac{1}{V_P}\int_P \epsilon_{ijk}\frac{\partial u_k}{\partial x_j} dV \\
&= \frac{1}{V_P}\epsilon_{ijk}\oint_P u_k n_j dA \\
&\approx \frac{1}{V_P}\epsilon_{ijk}\sum_{e' \in E'_P} \frac{u_k^e + u_k^f + u_k^c}{3} n_j^{e'} A_{e'} + \frac{1}{V_P}\epsilon_{ijk}\sum_{f' \in F'_P} \frac{u_k^P + u_k^e + u_k^f}{3} n_j^{f'} A_{f'},
\end{aligned} \tag{A.2}$$

where $V_P = \sum_{t' \in T'_P} V_{t'}$ is the volume of node P, e' is an index for the sub-edges, E'_P is the total number of sub-edges of node P, f' is an index for the boundary sub-faces and F'_P is the total number of boundary sub-faces associated with node P. The unit sub-edge $n_i^{e'}$ and sub-face $n_i^{f'}$ normals are pointing outwards with respect to P. The sub-edge $A_{e'}$ and sub-face $A_{f'}$ areas are also present (see typical shaded areas in Fig. A.1). It is important to note that the last term in the above equations is nonzero only when node P is a boundary node.

The Laplacian operator (left hand side of the stream vector Poisson equations) is constructed using the divergence theorem and the sub-edge concept as

$$\begin{aligned}
-\int_P \nabla^2 \psi_i dV &= -\oint_P \frac{\partial \psi_i}{\partial x_j} n_j dA \\
&\approx -\sum_{e' \in E'_P} \frac{\partial \psi_i}{\partial x_j}\Big|_{e'} n_j^{e'} A_{e'} - \sum_{f' \in F'_P} \frac{\partial \psi_i}{\partial x_j}\Big|_{f'} n_j^{f'} A_{f'},
\end{aligned} \tag{A.3}$$

where the last term is active only when node P is a boundary node. The required gradient operator for each sub-edge is constructed to satisfy the following set of equations

$$\left.\frac{\partial \psi_i}{\partial x_j}\right|_{e'} x_j^{PB} = \psi_i^{PB} \tag{A.4a}$$

$$\left.\frac{\partial \psi_i}{\partial x_j}\right|_{e'} x_j^{EF} = \psi_i^{EF} \tag{A.4b}$$

$$\left.\frac{\partial \psi_i}{\partial x_j}\right|_{e'} x_j^{EC} = \psi_i^{EC}, \tag{A.4c}$$

where x_j^{XX} are the simple average expressions

$$x_j^{PB} = x_j^B - x_j^P \tag{A.5a}$$

$$x_j^{EF} = x_j^f - x_j^e \qquad x_j^f = \frac{1}{N_F}\sum_{nof} x_j^{nof} \qquad x_j^e = \frac{1}{2}(x_j^B + x_j^P) \tag{A.5b}$$

$$x_j^{EC} = x_j^c - x_j^e \qquad x_j^c = \frac{1}{N_C}\sum_{noc} x_j^{noc}. \tag{A.5c}$$

Similarly ψ_i^{XX} are the simple average operators (since node values of ψ_i are to be solved)

$$\psi_i^{PB} = \psi_i^B - \psi_i^P \tag{A.6a}$$

$$\psi_i^{EF} = \psi_i^f - \psi_i^e \qquad \psi_i^f = \frac{1}{N_F}\sum_{nof} \psi_i^{nof} \qquad \psi_i^e = \frac{1}{2}(\psi_i^B + \psi_i^P) \tag{A.6b}$$

$$\psi_i^{EC} = \psi_i^c - \psi_i^e \qquad \psi_i^c = \frac{1}{N_C}\sum_{noc} \psi_i^{noc}. \tag{A.6c}$$

Nodes P and B are the two nodes associated with the edge of the sub-edge e', the index nof runs over all the nodes of the face (in total N_F) associated with the sub-edge e', and the index noc runs over all the nodes of the cell (in total N_C) associated with this sub-edge. We can analytically solve for the sub-edge gradient operators and get the following relations in compact matrix form

$$\begin{bmatrix} \left.\frac{\partial \psi_i}{\partial x_1}\right|_{e'} \\ \left.\frac{\partial \psi_i}{\partial x_2}\right|_{e'} \\ \left.\frac{\partial \psi_i}{\partial x_3}\right|_{e'} \end{bmatrix} = \frac{1}{\boldsymbol{x}^{PB} \cdot (\boldsymbol{x}^{EF} \times \boldsymbol{x}^{EC})} \begin{bmatrix} \left[\boldsymbol{x}^{EF} \times \boldsymbol{x}^{EC}\right] \\ \left[\boldsymbol{x}^{EC} \times \boldsymbol{x}^{PB}\right] \\ \left[\boldsymbol{x}^{PB} \times \boldsymbol{x}^{EF}\right] \end{bmatrix} \begin{bmatrix} \psi_i^{PB} \\ \psi_i^{EF} \\ \psi_i^{EC} \end{bmatrix}. \tag{A.7}$$

The boundary part of the Laplacian operator is a summation over sub-faces, and will be nonzero at boundary nodes only. In what follows we provide discrete forms for the coupled and segregated boundary conditions defined in section 4.3.

For the coupled method, discretisation of (35) leads to

$$n_\alpha \psi_\alpha^P \frac{V_P}{A_P} + n_\beta \psi_\beta^P \frac{V_P}{A_P} + n_\gamma \psi_\gamma^P \frac{V_P}{A_P} = 0 \tag{A.8a}$$

$$-\frac{\partial \psi_\beta}{\partial x_j}\Big|_{f'} n_j^{f'} A_{f'} = -\frac{\partial \psi_j}{\partial x_\beta}\Big|_{f'} n_j^{f'} A_{f'} + \epsilon_{\beta jk} \frac{u_k^P + u_k^e + u_k^f}{3}\Big|_{f'} n_j^{f'} A_{f'} \tag{A.8b}$$

$$-\frac{\partial \psi_\gamma}{\partial x_j}\Big|_{f'} n_j^{f'} A_{f'} = -\frac{\partial \psi_j}{\partial x_\gamma}\Big|_{f'} n_j^{f'} A_{f'} + \epsilon_{\gamma jk} \frac{u_k^P + u_k^e + u_k^f}{3}\Big|_{f'} n_j^{f'} A_{f'}, \tag{A.8c}$$

where $A_P = \sum_{f' \in F'_P} A_{f'}$ is the boundary area associated with boundary node P. The first equation is scaled by a factor so that it will be of the same order with the remaining two equations. The above equations consist the coupled form, where the stream vector components appearing in both sides of the equations are considered unknown. Equations (A.8b), (A.8c) are substituted in (A.3), while (A.8a) is used to replace the entire α component of the Poisson equation at the boundary.

For the segregated method, discretisation of (36) leads to

$$\psi_\alpha^P = -\frac{n_\beta}{n_\alpha}\psi_\beta^P - \frac{n_\gamma}{n_\alpha}\psi_\gamma^P \tag{A.9a}$$

$$-\frac{\partial \psi_\beta}{\partial x_j}\Big|_{f'} n_j^{f'} A_{f'} = \epsilon_{\beta jk} \frac{u_k^P + u_k^e + u_k^f}{3}\Big|_{f'} n_j^{f'} A_{f'} + \epsilon_{\alpha jk} \frac{\partial \psi_\gamma}{\partial x_k}\Big|_{f'} n_j^{f'} A_{f'} - \epsilon_{\gamma jk} \frac{\partial \psi_\alpha}{\partial x_k}\Big|_{f'} n_j^{f'} A_{f'} \tag{A.9b}$$

$$-\frac{\partial \psi_\gamma}{\partial x_j}\Big|_{f'} n_j^{f'} A_{f'} = \epsilon_{\gamma jk} \frac{u_k^P + u_k^e + u_k^f}{3}\Big|_{f'} n_j^{f'} A_{f'} + \epsilon_{\beta jk} \frac{\partial \psi_\alpha}{\partial x_k}\Big|_{f'} n_j^{f'} A_{f'} - \epsilon_{\alpha jk} \frac{\partial \psi_\beta}{\partial x_k}\Big|_{f'} n_j^{f'} A_{f'} \tag{A.9c}$$

On the boundary nodes, we replace the entire α component of (A.3) with (A.9a). We substitute (A.9b), (A.9c) into the β and γ components of (A.3) respectively. The Poisson equations are solved in succession where for the stream vector components appearing in the right hand side of (A.9a), (A.9b), (A.9c) the most recent values are used. An iterative scheme is used until the Poisson equations and boundary conditions are satisfied at an acceptable level.

The required gradient operator at each sub-face (right hand side of equations (A.8) and (A.9)) is constructed to satisfy the following set of equations

$$\frac{\partial \psi_j}{\partial x_i}\Big|_{f'} x_i^{PB} = \psi_j^{PB} \tag{A.10a}$$

$$\frac{\partial \psi_j}{\partial x_i}\Big|_{f'} x_i^{PF} = \psi_j^{PF} \tag{A.10b}$$

$$\frac{\partial \psi_j}{\partial x_i}\Big|_{f'} x_i^{PI} = \psi_j^{PI}, \tag{A.10c}$$

where $x_i^{PF} = x_i^f - x_i^P$, $x_i^{PI} = x_i^I - x_i^P$ and similarly $\psi_j^{PF} = \psi_j^f - \psi_j^P$, $\psi_j^{PI} = \psi_j^I - \psi_j^P$. Nodes P and B are on the edge associated with the boundary sub-face f', I (for Internal) is the node along the edge of P that is not part of the boundary face, but is still part of the internal cell that contains the boundary face (see Fig. A.1). We can analytically solve for the sub-face gradient operators and get the following relations in compact matrix form

$$\begin{bmatrix} \frac{\partial \psi_j}{\partial x_1}\Big|_{f'} \\ \frac{\partial \psi_j}{\partial x_2}\Big|_{f'} \\ \frac{\partial \psi_j}{\partial x_3}\Big|_{f'} \end{bmatrix} = \frac{1}{\boldsymbol{x}^{PB} \cdot (\boldsymbol{x}^{PF} \times \boldsymbol{x}^{PI})} \begin{bmatrix} \left[\boldsymbol{x}^{PF} \times \boldsymbol{x}^{PI}\right] \\ \left[\boldsymbol{x}^{PI} \times \boldsymbol{x}^{PB}\right] \\ \left[\boldsymbol{x}^{PB} \times \boldsymbol{x}^{PF}\right] \end{bmatrix} \begin{bmatrix} \psi_j^{PB} \\ \psi_j^{PF} \\ \psi_j^{PI} \end{bmatrix} . \tag{A.11}$$

This completes the treatment of the boundary terms.

References

[1] S. V. Apte, K. Mahesh, P. Moin, and J. C. Oefelein. Large-eddy simulation of swirling particle-laden flows in a coaxial-jet combustor. *International Journal of Multiphase Flow*, 29(8):1311–1331, 2003.

[2] B. Aupoix, S. C. Kassinos, and C. A. Langer. Asbm-bsl: An easy access to the structure based model technology. In *Progress in Wall Turbulence: Understanding and Modeling*, pages 277–285. Springer, 2011.

[3] S. Balay, M. F. Adams, J. Brown, P. Brune, K. Buschelman, V. Eijkhout, W. D. Gropp, D. Kaushik, M. G. Knepley, L. C. McInnes, K. Rupp, B. F. Smith, and H. Zhang. PETSc users manual. Technical Report ANL-95/11 - Revision 3.4, Argonne National Laboratory, 2013.

[4] S. Balay, M. F. Adams, J. Brown, P. Brune, K. Buschelman, V. Eijkhout, W. D. Gropp, D. Kaushik, M. G. Knepley, L. C. McInnes, K. Rupp, B. F. Smith, and H. Zhang. PETSc Web page. `http://www.mcs.anl.gov/petsc`, 2014.

[5] S. Balay, W. D. Gropp, L. C. McInnes, and B. F. Smith. Efficient management of parallelism in object oriented numerical software libraries. In E. Arge, A. M. Bruaset, and H. P. Langtangen, editors, *Modern Software Tools in Scientific Computing*, pages 163–202. Birkhäuser Press, 1997.

[6] M. Darwish, I. Sraj, and F. Moukalled. A coupled finite volume solver for the solution of incompressible flows on unstructured grids. *Journal of Computational Physics*, 228(1):180–201, 2009.

[7] D. G. Grigoriadis, C. A. Langer, and S. C. Kassinos. Diagnostic properties of structure tensors in turbulent flows. *Direct and Large-Eddy Simulation VII*, pages 41–47, 2010.

[8] F. Ham and G. Iaccarino. Energy conservation in collocated discretization schemes on unstructured meshes. *Annual Research Briefs*, 2004:3–14, 2004.

[9] F. Ham, K. Mattsson, and G. Iaccarino. Accurate and stable finite volume operators for unstructured flow solvers. *Annual Research Briefs, Center for Turbulence Research, NASA Ames/Stanford University*, pages 243–261, 2006.

[10] N. Kanaris, D. G. Grigoriadis, and S. C. Kassinos. Three dimensional flow around a circular cylinder confined in a plane channel. *Physics of Fluids (1994-present)*, 23(6):064106, 2011.

[11] S. C. Kassinos and E. Akylas. Advances in particle representation modeling of homogeneous turbulence. from the linear prm version to the interacting viscoelastic iprm. In *New Approaches in Modeling Multiphase Flows and Dispersion in Turbulence, Fractal Methods and Synthetic Turbulence*, pages 81–101. Springer, 2012.

[12] S. C. Kassinos, B. Knaepen, and D. Carati. The transport of a passive scalar in magnetohydrodynamic turbulence subjected to mean shear and frame rotation. *Physics of Fluids (1994-present)*, 19(1):015105, 2007.

[13] S. C. Kassinos, C. A. Langer, S. L. Haire, and W. C. Reynolds. Structure-based turbulence modeling for wall-bounded flows. *International Journal of Heat and Fluid Flow*, 21(5):599–605, 2000.

[14] S. C. Kassinos, C. A. Langer, G. Kalitzin, and G. Iaccarino. A simplified structure-based model using standard turbulence scale equations: computation of rotating wall-bounded flows. *International Journal of Heat and Fluid Flow*, 27(4):653–660, 2006.

[15] S. C. Kassinos and W. C. Reynolds. *A structure-based model for the rapid distortion of homogeneous turbulence*. PhD thesis, Thermosciences Division, Department of Mechanical Engineering, Stanford University, 1995.

[16] S. C. Kassinos, W. C. Reynolds, and M. M. Rogers. One-point turbulence structure tensors. *Journal of Fluid Mechanics*, 428(1):213–248, 2001.

[17] C. A. Langer and W. C. Reynolds. *A new algebraic structure-based turbulence Model for rotating wall-bounded flows*. PhD thesis, Thermosciences Division, Department of Mechanical Engineering, Stanford University, 2003.

[18] K. Mahesh, G. Constantinescu, S. V. Apte, G. Iaccarino, F. Ham, and P. Moin. Progress toward large-eddy simulation of turbulent reacting and non-reacting flows in complex geometries. *Annual Research Briefs, Center for Turbulence Research, NASA Ames/Stanford University*, pages 115–142, 2002.

[19] K. Mahesh, G. Constantinescu, and P. Moin. A numerical method for large-eddy simulation in complex geometries. *Journal of Computational Physics*, 197(1):215–240, 2004.

[20] S. V. Poroseva, S. C. Kassinos, C. A. Langer, and W. C. Reynolds. Structure-based turbulence model: Application to a rotating pipe flow. *Physics of Fluids (1994-present)*, 14(4):1523–1532, 2002.

[21] L. Quartapelle. *Numerical solution of the incompressible Navier-Stokes equations*, volume 113. Birkhäuser Verlag (Basel and Boston), 1993.

[22] W. C. Reynolds, C. A. Langer, and S. C. Kassinos. Structure and scales in turbulence modeling. *Physics of Fluids (1994-present)*, 14(7):2485–2492, 2002.

[23] M. M. Rogers and P. Moin. The structure of the vorticity field in homogeneous turbulent flows. *Journal of Fluid Mechanics*, 176:33–66, 1987.

[24] D. You, F. Ham, and P. Moin. Discrete conservation principles in large-eddy simulation with application to separation control over an airfoil. *Physics of Fluids (1994-present)*, 20(10):101515, 2008.